

A11A

NAG9-239

7N-25-CR

292196

398

The Solubility of Carbon Dioxide in Rhyolitic Melts:

A Quantitative FTIR Study

Robert A. Fogel and Malcolm J. Rutherford

Department of Geological Sciences, Brown University, Providence, Rhode Island 02912

February 14, 1989

(NASA-CR-186774) THE SOLUBILITY OF CARBON
DIOXIDE IN RHYOLITIC MELTS: A QUANTITATIVE
FTIR STUDY (Brown Univ.) 39 p

N90-70825

Unclass
00/25 0292196

1139 APR 23 A 9:54

Submitted to Am. Miner

Abstract

The solubility of CO_2 in rhyolite liquid has been determined using quantitative fourier transform infrared spectroscopy. Experiments were conducted along the 950°C , 1050°C and 1150°C isotherms and at pressures between 500 to 6600 bars under CO_2 saturated conditions. The 2350 cm^{-1} band which represents the antisymmetric stretch of dissolved CO_2 molecules, was used for quantitative CO_2 concentration determinations.

The 1050°C isotherm was investigated in greatest detail. Along this isotherm CO_2 solubility is ideal (in the Henrian sense) up to roughly 2300 bars. Above this pressure deviations from ideality are prominent, with concentrations less than predicted by extrapolation of the linear form of Henry's Law. The effect of increasing temperature is to decrease the solubility of molecular CO_2 . Similar behavior has been found in albite (Stolper et al., 1988). The water content of these glasses were also monitored using the 3570 cm^{-1} OH^- fundamental vibration. Maximum H_2O contents were 0.30 wt % and the presence of these small amounts of H_2O apparently has no effect on CO_2 solubility.

The behavior of CO_2 solubility in rhyolite over the entire P-T range investigated can be modeled with a modified or non-linear Henry's Law equation. This expression requires the selection of a reference T and P and the data can be regressed to determine the partial molar volume (\bar{v}) of dissolved CO_2 as well as its heat of solution (Δh). Regression of the data presented gives a value of $34.0 \pm 0.5\text{ cm}^3/\text{mole}$ for \bar{v} and $-15.9 \pm 3.9\text{ kJ/mole}$ for Δh where the reference P and T are 2025 bars and 1050°C .

Samples retained their original shapes throughout the experiments. This, as well as the detection of CO_2 diffusion profiles in various samples, indicates that the approach to equilibrium was limited solely by the process of diffusion. The melt viscosities were apparently high enough to hinder $\text{CO}_2(\text{fluid})$ -melt equilibration by silicate mixing. The diffusion coefficient of CO_2 in rhyolite at 1050°C was estimated in three charges to be $2.362 (\pm 0.485) \times 10^{-8}\text{ cm}^2/\text{mole}$. in close agreement with the work of Watson et al., (1982) on CO_2 diffusion in silicate melts of somewhat different composition.

Infrared bands attributable to dissolved carbonate complexes were not detected under any of the experimental conditions. This appears to be consistent with the general decrease in the CO_3^{2-} to CO_2 (Molecular) ratio in the petrogenetic sequence basalt, andesite, rhyodacite, rhyolite investigated in this lab. Basalt, the most primitive composition, dissolves CO_2 solely in the form of carbonate complexes whereas the highly evolved member of this sequence, rhyolite, dissolves CO_2 exclusively in the molecular form. A comparison of this new data for CO_2 solubility in rhyolite, with data for CO_2 solubility in basalt (Stolper and Holloway, 1988) shows that both on a mole fraction and weight percent basis, slightly more CO_2 dissolves into rhyolite than into basalt. The contention of many workers that CO_2 is more soluble in mafic magmas than it is in more evolved compositions is clearly incorrect.

Introduction

Magma genesis and evolution is often associated with a volatile phase in which carbon dioxide is an important component. The work of Roeder (1965), Gerlach (1986), Dixon et al., (1988) and others have demonstrated that CO_2 is the main component of the fluid phase likely to develop in basaltic magma. Although water is an important component in more silicic magmas, CO_2 is present in significant amounts and plays a critical role in the genesis of high silica magmas. For example: Johnson and Rutherford (1989) and Rutherford et al., (1985) have shown that the presence of CO_2 in the fluid phase associated with the Fish Canyon Tuff quartz latite and the 1980 Mount St. Helens dacite dramatically affected phase stability and occurrence in these magmatic events, respectively

Although the role of carbon dioxide in magmatic processes has long been considered to be an important one, current understanding of the physicochemical effects of CO_2 upon magma is still in its infancy. This appears to be an extension of the poor state of knowledge of the gaseous properties of carbon dioxide, where the non-ideality of CO_2 at high pressures and temperatures is still poorly known and the behavior of CO_2 in the presence of other magmatic gases is even less well understood.

With regards to magmatic evolution, the thermodynamic property of CO_2 of greatest importance is its solubility within silicate liquid compositions. A detailed understanding of processes such as phase equilibrium, magma vesiculation, bubble growth, magma explosivity as well as planetary atmospheric evolution, all require reasonable estimates of the ability of silicate liquids to accommodate CO_2 in solution. An understanding of CO_2 speciation within the silicate molecular structure is also of importance, as it leads to physically correct solution models and more accurate magma- CO_2 solubility predictions.

Although the significance of CO_2 solubility measurements has long been recognized, advances in this area were hindered by the lack of a reliable technique for measuring CO_2 concentrations. As a consequence, most studies of CO_2 solubility were carried out at very high pressure (> 10 kb) where CO_2 solubility is appreciable, thus, increasing the accuracy of existing analytical methods.

The work of Fine and Stolper, (1985) made the first extensive use, in petrology, of quantitative infrared spectroscopy (QIS) for determining CO₂ concentrations in geological glass compositions. QIS is a rapid, non-destructive technique with the capability of high spatial and compositional resolution. Currently, QIS has only been applied to CO₂ solubility measurements under limited conditions of pressure, temperature and composition. Stolper et al., (1987) studied the solubility behavior of CO₂ in albitic glass at temperatures between 1450°C and 1625°C and Stolper and Holloway, (1988) determined the Henry's Law behavior of CO₂ in basaltic glass at 1200°C and at pressures below 1500 bars.

The subject of this study is the determination of CO₂ solubility in rhyolite glass under a wide range of P and T. Our analytical method makes use of quantitative FTIR spectroscopy for determining both CO₂ solubility and speciation (molecular CO₂ vs carbonate). Experiments were carried out at pressures between 500 and 6600 bars and at temperatures between 950°C and 1150°C. These conditions cover a pressure range where Henry's Law is adhered to as well as higher P conditions displaying significant deviations in Henry's Law behavior. Additionally, the range in temperature allows for the extrapolation of results to lower T as well as direct application to high temperature rhyolitic volcanism. This T-P range also allows a comparison of our work with that of Stolper and Holloway, (1989) to address the common perception that CO₂ solubility is much greater in liquids of low silica activity, (basalt), than liquids of high silica activity (rhyolite) (eg. Eggler and Rosenhauer, 1978; Carmichael et al., 1974)

Experimental Techniques

Experimental Procedure

Rhyolitic Obsidian VNM50-15 from the Brown University collection was used in all experimental runs. VNM50-15 is an obsidian fragment found in a stream bed of the Valles Caldera, New Mexico, area. It is vitreous and free of both vapor bubbles and silicate crystals (although occasional crystals of Fe-Ti oxides on the order of a few microns are present). Its chemical composition is that of a highly evolved rhyolite and is quite similar to that of other

rhyolitic obsidian flows found in that area (Fogel and Rutherford, 1989). Table 1 gives electron microprobe chemical analyses of sample VNM50-15 as well as its CIPW norm. Normalized to the granite ternary (quartz-albite-orthoclase) VNM50-15 falls quite close to the 3000 bar H₂O saturated granite minimum melting point (Tuttle and Bowen, 1960). The H₂O content of VNM50-15 as determined by IR analyses is 1300 ppm by weight (ppmw).

Rectangular chips of VNM50-15 glass were cut with a diamond saw and ground to a weight of between 50 to 150 mg. These chips were weighed and placed in Ag₇₀Pd₃₀ tubes welded shut at the bottom. Silver oxalate (Ag₂C₂O₄) was then added to the tube in an amount far in excess of that required to saturate the sample in CO₂. The tube was welded shut and tested for leaks by weighing the tube, heating to 112°C for a few minutes, and then rapidly quenching in water. Leakage of the tube was noted by reweighing the tube and checking for a water weight gain.

Samples were run in either TZM pressure vessels or an internally heated pressure vessel (IHPV). The TZM bombs were used to investigate the low pressure region below 3000 bars and temperatures below 1100°C. The internally heated pressure vessel was used for pressures greater than 3000 bars and/or temperatures in excess of 1100°C. The pressurizing medium for both vessels was argon. For the TZM experiments, pressure was measured on a 0-7000 bar bourdon tube Heise gauge periodically calibrated at the factory. For IHPV experiments, runs between 3000 and 6000 bars were measured on a 0 to 6900 bar THI transducer calibrated at the factory. Runs in excess of 6000 bars were measured for pressure on a 0 to 13,800 bar Foxboro manganin cell calibrated at the factory. Both of these pressure measuring devices were periodically checked against the Heise gauge for internal consistency.

Run temperatures were controlled by Eurotherm temperature controllers accurate to within $\pm 3^\circ\text{C}$. In the IHPV experiments, the charge sat in a cylindrical platinum container the walls of which are 1 mm thick. Pt-Pt₉₀Rh₁₀ measuring and controlling thermocouples were inserted into a hole in the bottom of this container. This platinum block assembly was used in order to minimize temperature gradients across the sample. The run temperature is considered to be within $\pm 5^\circ\text{C}$ of that recorded. The TZM assembly consisted of a TZM alloy bomb with an

external sheath. A few bars of Ar pressure were constantly applied between the bomb and the sheath to prevent TZM oxidation. As a consequence of this type of assembly, temperatures within the bomb could not be measured during the course of the experiment. Temperatures within the bomb were, thus, calibrated at 1 atm Ar pressure against the temperature in the sheath wall. The reproducibility of this calibration is $\pm 5^{\circ}\text{C}$. TZM run temperatures are thought to be accurate to better than $\pm 10^{\circ}\text{C}$.

IHPV runs were quenched by turning the power off and rotating the vessel 90° to disturb the thermal stability of the bomb. Quench rates were on the order of $100^{\circ}\text{C}/\text{sec}$ for the first 2-3 seconds of the quench. The TZM runs were quenched by removing the bomb from the furnace and quenching in water. After the run, the charges were weighed to check for weight loss. Upon cutting of the noble metal container, an audible "hiss" ascertained the presence of a CO_2 vapour phase and the integrity of the capsule during the run. Experimental glasses were also examined under a binocular microscope for the presence of vapour bubbles, the presence of which lends support for the existence of a vapour phase during the run.

FTIR Sample Preparation and Analytical Technique

After preliminary examination, experimental glasses were wafered and ground in a slurry of alumina and water. Samples were generally ground to between 100 and $300\ \mu\text{m}$, the thickness depending on the amount of CO_2 suspected to be in solution in the sample and the resolution desired (see Quantitative IR section below.) Samples were polished on both sides to a grit of either 0.3 or $0.05\ \mu\text{m}$. FTIR sections were then examined under a microscope and a sketch of the section made. Section thicknesses were mapped using a Mitutoyo digital dial indicator with a precision of roughly $\pm 3\ \mu\text{m}$. This "mapping" was necessary because of the difficulty of making sections of uniform thicknesses. The fine spatial resolution of the micro-FTIR puts added emphasis on determining sample thickness. An "average thickness" may lead to erroneous concentration determinations when spatial resolution is on the order of tens of microns.

FTIR spectra were performed on the Brown University IBM Instruments Model IFS-100 FTIR spectrometer. All samples were analysed with the instruments micro-FTIR attachment.

The microscope is equipped with a 15 X magnification objective lense. A set of apertures ranging in size from 1200 μm to 300 μm provided spatial resolution from 80 to 20 microns, respectively. Samples were positioned on top of apertures on a sample holder slide. This assembly was placed on the microscope stage and an area free or relatively free of bubbles was selected for analyses. Spectra were taken using a globar source, a HgCdTe detector, a 4 cm^{-1} resolution and either 128, 256, or 512 scans.

Quantitative IR Spectroscopy

The relationship between concentration and IR band intensity is given by the Beer-Lambert law:

$$C = 10^6 \frac{(MW)(\text{Abs})}{(\rho)(\epsilon)(d)} \quad (1)$$

where C is concentration in ppm by weight, MW is the molecular weight of the IR active component, Abs is the band intensity in dimensionless absorbance units, ρ is sample density in g/l, ϵ is the molar absorbtivity or extinction coefficient of the IR band in L/(mole-cm), and d is the thickness of sample under the IR beam in cm.

Abs is measured from peak to baseline where the baseline is interpolated from the surrounding spectral range. Baseline interpolation is accomplished by drawing a line tangential to the baseline on both the high and low energy side of the band. In cases where silicate network vibrations overlap the band of interest or interfere with the smooth interpolation of baseline, spectral subtraction of a reference sample devoid of the absorbing species of interest is used; the spectra of the reference being first normalized to the thickness of the unknown. Since the bands of interest in the present study have smooth non-complicated background, spectral subtraction was generally not employed.

The density of VNM50-15 was measured using a 25 ml pycnometer. Water was used as the liquid density medium, being first boiled and set to cool to 25°C to eliminate dissolved oxygen. A density of 997.05 g/L (CRC Handbook of Chemistry and Physics, 1981) was taken as the density of deionized H₂O at 25°C to which the glass densities were referenced. The density of 7 chips of

VNM50-15 cumulatively weighing 0.89083 g was determined to be 2348 ± 10 g/L. All CO₂ solubility measurements were determined with this value. The net increase in the CO₂ content of the experimental melts was assumed to have a negligible affect on sample density.

An example of a typical FTIR spectra of a CO₂ bearing rhyolite is shown in Figure 1. The spectral range of interest is the area between 5000 cm^{-1} and 1000 cm^{-1} . As displayed in Figure 1, CO₂ bearing rhyolitic melts contain a number of bands in this spectral region. Each of these bands will be discussed individually.

The 1375 and 1610 cm^{-1} Bands. These doublet bands centered around the 1375 and 1610 cm^{-1} areas are due to the presence of carbonate (CO_3^{2-}) bonded to the silicate network. CO₂ in the form of carbonate appears to be the dominant form of CO₂ dissolution into basaltic, diopsidic and akermanitic melts (Fine and Stolper, 1986; Rai et al., 1983; Sharma et al, 1979). At high pressures, it has been shown to be present in sodium aluminosilicate melts (Stolper et al., 1987; Fine and Stolper, 1985). Unpublished work from this laboratory show it to be an important species in andesitic (56 wt% SiO₂) and rhyodacitic (66 wt % SiO₂) melts below 3 kb. None of the rhyolite experiments done in this study show the presence of any carbonate bands. Spectral subtraction of standard CO₂ devoid material show a flat pattern in this area suggesting that if CO₂ dissolves as carbonate under the physical conditions covered by this study, it is present in amounts below FTIR detectibility: ≈ 25 ppm (Fine and Stolper, 1985).

The 1600 and 1820 cm^{-1} Bands. Newman et al., (1986) attributed these bands to aluminosilicate network vibrations. Their work involved rhyolitic compositions similar to that of this study. They found these bands to be uncorrelated with water content. The current study shows no correlation of the intensity of these bands with CO₂ content. FTIR spectra of the compositional sequence: basalt (49 wt% SiO₂), andesite (56 wt% SiO₂), rhyodacite (66 wt% SiO₂) and rhyolite (76 wt% SiO₂) show a clear growth of these bands. They are barely existent in the basaltic samples, but become more clearly present and well defined higher up in the sequence. Although most silicate network vibrations are present at energy levels below 1200 cm^{-1} , the combination of factors listed above tend to support the suggestion of Newman et al., (1986). We

suggest, however, due to the high energy levels of these bands, that they may be combination or overtones bands of the aluminosilicate network.

The 2287 cm⁻¹ Band. This band has been assigned to the ν_3 antisymmetric stretch of ¹³CO₂ molecules (Stolper et al., 1987; Fine and Stolper, 1985). It appears as a small band just off the shoulder of the high intensity band centered at 2350 cm⁻¹. Stolper et al., (1987) determined the extinction coefficient of this band (ϵ_{2287}) for molecular CO₂ in albite glass. Their value for ϵ_{2287} of 11.7 L/(mole-cm) was determined for the *total* CO₂(Molecular) in albite melt rather than the molecular ¹³CO₂ it represents. At low CO₂ concentrations, this band is not very intense and, thus, is generally most useful for the determination of high CO₂ concentrations.

The 2350 cm⁻¹ Band. This band represents the ν_3 antisymmetric stretch of dissolved ¹²CO₂ molecules (Fine and Stolper, 1985). It is a sharp narrow band that is often the dominant feature in the spectrum under moderate to high CO₂ concentrations. Its extinction coefficient in sodium aluminosilicate melts has been determined by Fine and Stolper, (1985). They investigated the speciation of CO₂ along the join NaAlO₂-SiO₂ studying the glass compositions NaAlSi₂O₆ (jadeite), NaAlSi₃O₈ (albite) and NaAlSi₄O₁₀. A single value for ϵ_{2350} of 945 ± 45 L/(mole-cm) was determined for all three compositions.

The 2350 cm⁻¹ band is used in this study as the principle band for the determination of CO₂ solubility in rhyolitic compositions. Since the only calibration for ϵ_{2350} in silicate compositions is for the join NaAlO₂-SiO₂, there is some concern that the value of 945 L/(mole-cm) may not be appropriate to rhyolitic compositions. There is, however, reason to believe that the value of ϵ_{2350} established for the NaAlO₂-SiO₂ join is either directly applicable or quite close to that of ϵ_{2350} in rhyolite. As mentioned previously, Fine and Stolper (1985) showed that within the sodium-aluminosilicate join they investigated, ϵ_{2350} was not a function of SiO₂ concentration. In addition, the composition NaAlSi₄O₁₀ in their study is roughly that of the 1 atm albite-silica eutectic. The addition of orthoclase to the albite-silica system produces the granite ternary into which sample VNM50-15 projects with less than a 3% residual (Table 1). The combination of these factors suggest that the only influence, if any, on changing ϵ_{2350} for rhyolitic compositions

from that determined for the sodium-aluminosilicates, is the presence of K_2O substituting for Na_2O in the silicate structure. The addition of minute amounts of FeO , MgO , MnO , TiO_2 and CaO which total to no more than 3% is unlikely to have an effect on ϵ_{2350} .

The question then stands at: does the replacement of K_2O for Na_2O in the aluminosilicate melt alter the value of ϵ_{2350} ? Because of the broad similarities of K_2O and Na_2O , a case can be made that ϵ_{2350} is little affected by this substitution. It is more intuitively satisfying, however, to note that the species under discussion is dissolved in the silicate melt in the molecular form—ie. CO_2 is "trapped" in holes in the melt and is not "bonded" to the aluminosilicate network. An alkali substitution is likely to have a lesser affect for a dissolved molecular species which would be responding to changes in the size and shape of the "holes" they occupy than species bonded to the network which would respond to changes in the composition and structure of the network. The works of Silver and Stolper, (1989) on albite glass and Newman et al., (1986) on rhyolite glass which look at the nature and solubility of water seem to support this idea. The extinction coefficients reported by these authors for the H_2O band associated solely with hydroxyl (4500 cm^{-1}) are 1.73 and 1.13 L/(mole-cm), whereas the extinction coefficients for the bands representing molecular H_2O are: $1630\text{ cm}^{-1} = 55$ and 49 L/(mole-cm) and $5200\text{ cm}^{-1} = 1.61$ and 1.67 L/(mole-cm) for rhyolite and albite glass, respectively.

Ultimately, the value of the extinction coefficient used in the Beer-Lambert Law affects only the magnitude of CO_2 solubility. CO_2 concentrations determined relative to each other are not dependant upon ϵ and can be used with confidence. If indeed ϵ_{2350} is shown to be significantly different in rhyolite than in albite glass, absolute CO_2 concentrations can be redetermined with the Beer-Lambert law and the updated value of ϵ_{2350} .

The 3570 cm^{-1} Band. The fundamental OH stretching vibration produces this broad band (Nakamoto, 1986). Water, in the form of both $H_2O_{(Molecular)}$ and OH contribute to the intensity of this band. It is centered around 3570 cm^{-1} and is highly assymmetric to the low energy side. This band is used in this study as the fundamental band for the determination of H_2O contents of the experimental glasses. The extinction coefficient for this band in rhyolitic glasses for water

contents of up to 2.64 wt % has been determined by Newman et al., (1986). They found that ϵ_{3570} was not constant with total water contents but rather, varied with the proportion of OH to H_2O . ϵ_{3570} was therefore modeled as:

$$\epsilon_{3570} = \epsilon_{OH,3570} X_{OH} + \epsilon_{H_2O,3570} X_{H_2O}$$

where X_{OH} and X_{H_2O} are the mole fraction of water in the OH and $H_2O_{(Molecular)}$ states relative to total water, respectively. $\epsilon_{OH,3570}$ and $\epsilon_{H_2O,3570}$ are the extinction coefficients contributing to ϵ_{3570} for OH and $H_2O_{(Molecular)}$ and were determined to be 100 ± 2 L/(mole-cm) and 56 ± 4 L/(mole-cm), respectively. Since the total water contents of all experimental samples determined in this study were below 0.30 wt % and no molecular water bands were detected, we use $X_{OH} = 1$ and $\epsilon_{3570} = \epsilon_{OH,3570}$ for determining total water contents.

The 3710 cm^{-1} Band. Stolper et al., (1987) attribute this band to a combination of the ν_1 and ν_2 modes of $^{12}CO_2$. It is a low intensity band off the high energy shoulder of the 3570 cm^{-1} OH band. ϵ_{3710} was determined in their study to be 13.9 L/(mole-cm) in albite glass.

The 4500 cm^{-1} Band. This band was assigned to the combination mode of Si-OH groups by Stolper, (1982). Newman et al., (1986) determined a value of 1.73 for ϵ_{4500} in rhyolite glass. Although at these low water contents this band supplies the same information as does the 3570 cm^{-1} band, the latter is used instead of the former because of the much greater intensity of the 3570 cm^{-1} band.

The 4700 cm^{-1} Band. This band appears to be correlated to total CO_2 concentration. It is absent in the VNM50-15 starting material. At high CO_2 concentrations it appears as a roughly symmetric narrow band beginning only a few wavenumbers from the high energy baseline of the 4500 cm^{-1} band. To our knowledge this band has not been identified in IR spectra of geological melts. We tentatively assign it to the first overtone of the 2350 cm^{-1} $^{12}CO_2$ band.

Evaluation of Uncertainty

Precision. The Beer-Lambert law describes the proportionality between species concentration and IR band intensity, density and sample thickness. The effect of the uncertainty in each of

these variables contributes to the overall precision of the analyses. An uncertainty of $\pm 3 \mu\text{m}$ was assigned to the measured thickness, and a standard deviation of $\pm 10 \text{ g/L}$ was determined for the density measurements. To find the standard deviation of band intensity measurements, 12 spectra were taken on the same spot of sample BF-153C. A band intensity of 1.5032 was determined for the CO_2 peak at 2350 cm^{-1} with an absolute standard deviation of ± 0.0145 or a relative standard deviation of $\pm 0.96\%$. Considering only the uncertainty in band intensity, these measurements translate into a CO_2 concentration of $2926 \pm 28 \text{ ppmw}$. The precision of measured intensity is even better for the H_2O band at 3570 cm^{-1} where for the 12 spectra an average band intensity of 0.21809 was determined with an absolute standard deviation of ± 0.00152 or a relative standard deviation of 0.70% . This translates into a water content of $1643 \pm 11 \text{ ppmw}$.

If the uncertainty assigned to the thickness is treated as a standard deviation, this value along with the standard deviation in measured absorbance and density can be used to evaluate a total precision for measured concentration. The standard deviation of the measured concentration is then simply given by the square root of the sum of the squares of each of the relative standard deviations. When this is done a precision of between 1.3 and 3.2% is determined for CO_2 with the precision on measured H_2O content being nearly the same. The relative contribution to these values from greatest to least is thickness, density and absorbance; although the relative uncertainty in thickness changes dramatically with sample thickness. (In these calculations it was also assumed that the uncertainty in the measured absorbance of all other samples was identical to that of BF-153C. While this is surely a simplification, it is probably a good approximation for most of the measured concentration range.)

Accuracy. This is the hardest form of uncertainty to evaluate. It is contributed to by uncertainty in the extinction coefficient, sample inhomogeneity, and the lack of suitable standards of similar composition having CO_2 concentrations close to that of the unknowns. The lack of these types of standards is unaddressable at this time, although if these were available, the current research would probably not be needed. With regards to sample heterogeneity, very few samples were found to have random deviations in CO_2 concentrations; a condition which would allow

analyses of various areas of the sample to obtain an average composition. Almost all types of inhomogeneity were attributable to diffusion gradients. The procedure for determining equilibrium composition as well as a more detailed description of sample inhomogeneities is outlined below (see Kinetics of CO₂ Solubility). Nevertheless, 7 analyses were taken on 7 different places on the rim of sample BF-153 with sample thicknesses ranging from 97 to 106 μm . For CO₂, an average concentration of $2,605 \pm 92$ ppmw (3.5%) was determined and for H₂O, an average concentration of $1,652 \pm 60$ ppmw (3.6%) was obtained.

The value of the extinction coefficient of the 2350 cm^{-1} band has already been discussed. Fine and Stolper, (1985) assign a value of $945 \pm 45\text{ L}/(\text{mole}\cdot\text{cm})$ to this parameter. If the arguments presented previously for acceptance of this value as appropriate to rhyolitic compositions are taken, then the effect on the accuracy of CO₂ concentrations due to the uncertainty in ϵ_{2350} is quantifiable. The 45 cm^{-1} uncertainty in ϵ_{2350} can be readily translated into a relative standard deviation in CO₂ concentration of 4.76% (if the uncertainty of $\pm 45\text{ cm}^{-1}$ given by Stolper and Fine (1985) is a standard deviation on the value of ϵ_{2350}). Similarly, the relative standard deviation of measured H₂O content attributable to the uncertainty in ϵ_{3570} ($100 \pm 2\text{ cm}^{-1}$) is 2%.

Experimental Results

The Data

Results of CO₂-rhyolite experiments tabulated for each isotherm are presented in Table 2. The 1050°C isotherm was the most extensively studied and gives the most detailed information on both the Henry's Law region and the non-ideal (in the Henrian sense) region. The 950°C and 1150°C isotherms are most useful in delineating the effects of temperature on CO₂ solubility.

The Henry's Law Region

Figure 2 is a plot of the CO₂ concentration in ppmw vs CO₂ fugacity (f_{CO_2}) for the portion of the 1050°C isotherm adhering to Henry's Law. CO₂ fugacity's were calculated with the Hard Sphere Modified Redlich-Kwong equation of state of Kerrick and Jacobs, (1981). The figure shows

a highly correlated linear trend between f_{CO_2} and dissolved CO_2 up to a f_{CO_2} of 3531 bar ($P = 2025$ bar). The first evidence of non-ideality is seen in the $f_{\text{CO}_2} = 4977$ bar run ($P = 2490$ bar) indicating that non-ideality begins between 2025 and 2490 bars total pressure.

The Non-Ideal Region

The pressure region above which CO_2 solubility acts in a non-ideal manner begins at a pressure of roughly 2300 bars. This is portrayed in Figure 3 where f_{CO_2} is plotted against ppm (mole) CO_2 for the entire experimental pressure range. Above the $f_{\text{CO}_2} = 4977$ run, CO_2 solubility quickly becomes non-ideal, deviating sharply from the Henry's Law solubility relation. The overall pressure dependence is roughly linear at these pressures and temperatures (Figure 4).

Temperature Dependence

The experiments confirm a net decrease in CO_2 solubility with increasing temperature. This behavior is portrayed in Figures 3 and 4 where P and f_{CO_2} vs ppm CO_2 is contoured for temperature. This effect is similar to that observed by Stolper et al., (1988) for CO_2 solubility in albite glass.

CO_2 Solubility and H_2O Concentration

The H_2O concentration of all experimental glasses is quite low, generally ranging in the 1500 ppm (by wt.) level. Figure 5 displays the variation in water content with CO_2 concentration. The general appearance of the data plotted in Figure 5 suggests only a slight positive correlation between CO_2 and water concentration. Due to the generally low H_2O concentration of all glasses and the lack of a well defined correlation between CO_2 and H_2O concentrations we conclude that the CO_2 solubility measurements presented here are unaffected by the presence of dissolved H_2O .

The low H_2O concentration of the experimental glasses is due to the low initial H_2O concentration of the starting material (1300 ppm by wt.) as well as the conditions outside the capsule walls. As described previously, TZM experiments were carried out with an Ar gas pressurizing medium along with graphite filler rods exterior to the noble metal containers. Any H_2 entering the bomb from the exterior must first react with the graphite to form CH_4 ; a process that keeps the fugacity of H_2 exterior to the charge at a minimum. IHPV runs are also conducted

with an Ar pressurizing medium and H_2 gas is seldom introduced into the vessel. The overall $f_{O_2} \cdot f_{H_2}$ state of the Brown University IHPV system at run conditions appears to be somewhere between the Ni-NiO- H_2O and MnO-Mn $_3$ O $_4$ - H_2O buffers. This is attested to by the ease of maintaining H_2O within charges buffered at MnO-Mn $_3$ O $_4$ and the difficulty of maintaining charges buffered at Ni-NiO in phase equilibrium experiments. This implies that the IHPV apparatus is intrinsically oxidizing and/or contains little extraneous H_2 within the bomb. This process helped maintain a low f_{H_2} .

Although these techniques help keep total water at a reasonably low level, it raises the question of whether conditions within the noble metal capsule were too reducing; a condition that would produce substantial CO as well as CO $_2$. Several factors, however, lead us to believe this was not a substantial problem. First, many of the experimental glasses contained large bubbles of trapped gas. FTIR spectra taken of these bubbles (accompanied by a computer normalized subtracted spectra of a bubble free portion of the glass) showed a peak for gaseous CO $_2$. Similar spectra of bubbles in experimental rhyolitic glasses, run with graphite and silver oxalate, contain a peak centered about 2180 cm^{-1} that we attribute to gaseous CO. This suggests the relative absence of substantial gaseous carbon monoxide in the vapor phase. Second, if f_{O_2} conditions within the charge dropped too low, graphite would have precipitated. Graphite has not been observed in any of our experimental run products. Additionally, graphite-C-O gas equilibria puts constraints on the maximum amount of CO possibly present within the charge. Figure 6 is a plot of the mole % CO $_2$ in equilibrium with graphite and CO for the three isotherms investigated in this study. Graphite-C-O gas equilibria becomes richer in CO $_2$ with increasing P and decreasing T. As can be seen from the graph, for most of the 1050°C experiments the minimum allowable molar CO $_2$ content of the gas is greater than 70%. Since graphite has not been found in any of the experimental run, the molar CO $_2$ percentage of the gas phase delineated in Figure 6 represent minimum values.

Kinetics of CO $_2$ Solubility

The principal objectives of this study did not include the determination of the diffusion of CO $_2$

in rhyolite glass. After the initial experiments were conducted, it became obvious that CO_2 diffusion into the melt was the rate limiting step for the attainment of equilibrium. Mixing and flow of the melt at run temperature were not processes that enhanced the attainment of equilibrium. With few exceptions, experimental glasses were removed from their $\text{Ag}_{70}\text{Pd}_{30}$ capsules in the exact shape that they were cut. This phenomenon was sometimes so extreme that even the original saw marks were still present; albeit in a vitreous pristine state. This was undoubtedly due to the very high viscosity of rhyolitic melt. These observations imply that very little mixing of the melt occurred during the run and that the primary equilibrating mechanism was that of diffusion.

Many of the short term runs contained diffusion profiles. An inspection of Table 2 shows that most run durations were at least 48 hours. These long run durations along with the diffusion rate of CO_2 in rhyolite were enough to produce diffusion profiles that extended over many hundreds of microns into the glass and usually on the order of a millimeter or two. The resulting profiles were long and broad. In no case was a diffusion profile produced where the center CO_2 concentration reached 0—the amount of CO_2 in the VNM50-15 starting material (see Table 2). The core CO_2 concentration was almost always more than 1/3 the rim content. Diffusion proceeded into the melt from all sides. It is presumed that the high melt viscosity—described above—helped keep the vapour phase exposed to the entire exterior of the melt at all times.

For the runs that contained diffusion profiles, the CO_2 concentrations accepted as equilibrium concentrations were those of the rims. The spot size analyzed in all FTIR spectra was never greater than 80 μm . Rim compositions were, therefore, averages of roughly the outer 80 μm of the sample. In these cases, spectra were also taken of the second 80 μm away from the rims and were found to have CO_2 contents only trivially (a few percent if at all) smaller than the rim contents. One sample, BF-153, was found to have CO_2 concentrations that were higher in the core than at the rim. In this case, rim concentrations were still accepted as equilibrium concentrations. The cause of this reverse gradient is still not understood; however, both core (BF-153C) and rim (BF-153) compositions are presented in Table 2.

With the realization that these experiments were not optimally designed to extract diffusion information, certain simplifying assumptions can be made in order to extract a qualitative value for the diffusivity of CO₂ into rhyolitic melt at 1050°C. An optimally designed experiment would pay much closer attention to the geometry of the charge and more rigorously determine distances between analysed points.

We first assume that the charge geometry is that of a cylinder and that diffusion proceeds into the sample from all directions. Additionally it is assumed that the area of analyses is unaffected by diffusion into the liquid from the top and bottom of the cylinder. Having made these assumptions, knowledge of the run duration as well as the CO₂ concentration as a function of core and rim distance enable the calculation of diffusion coefficients. The method reported in Crank (1985) for diffusion into a cylinder is used. Table 3 gives core and rim CO₂ concentrations of three experimental runs as well as other relevant information required for the calculation of D_{1050°C}; the diffusion coefficient of CO₂ in rhyolite at 1050°C. The average value of D_{1050°C} for the three experiments is $2.362 (\pm 0.485) \times 10^{-8}$ cm²/sec or a Log D_{1050°C} of -7.63. These values compare very favorably with that of Watson et al, (1982) for diffusion of CO₂ into a sodium aluminosilicate of composition 60% SiO₂, 30% Na₂O and 10% Al₂O₃ by weight. Their expression for D, uncorrected for pressure (negligible at P-T discussed here, eg. 0.10 Log units at 1050°C and 500 bars), yields a Log D_{1050°C} of -7.25. In view of the approximations made here to retrieve Log D_{1050°C} the agreement between the two studies is excellent.

Thermodynamics of CO₂ Solubility

At extreme levels of dilution, the solubility of a component within a liquid obeys Henry's Law. For the solubility of CO₂ within a liquid it is given as:

$$f_{\text{CO}_2} = X_{\text{CO}_2} H \quad (2)$$

where f_{CO_2} is the fugacity of CO₂ in bars, X_{CO_2} is the mole fraction of CO₂ in the liquid and H is the Henry's Law constant at constant T. This equation expresses a linear relationship between CO₂ solubility and fugacity. Figure 2 shows that CO₂ solubility in rhyolite obeys this law quite

strictly up to approximately 2300 bars total pressure. The Henry's Law constant determined with a least squares regression of the data between 0 and 2000 bars for the 1050°C isotherm gives $H = 1.937 \times 10^6$ bar with a correlation coefficient (R^2) of 0.999. For this and all subsequent calculations, f_{CO_2} was determined with the Hard Sphere Modified Redlich Kwong (HSMRK) model of Kerrick and Jacobs (1982).

Above 2300 bars the linear form of Henry's Law (2) is no longer applicable and must be modified to take into account the effect of pressure. This may be accomplished with the thermodynamic equality:

$$(\delta \ln f_{\text{CO}_2} / \delta P)_{T,X} = \bar{v} / RT \quad (3)$$

to obtain the Krichevsky-Kasarnovsky equation (Prausnitz et al., 1986):

$$\ln f_{\text{CO}_2} / X_{\text{CO}_2} = \ln H + \bar{v}(P - P_r) / RT \quad (4)$$

where $H(P_r)$ is the Henry's Law constant at a reference pressure P_r and \bar{v} is the partial molar volume of CO_2 in the liquid. Similarly, the following thermodynamic equality can be used to modify Henry's Law to take into account changes in temperature:

$$(\delta \ln f_{\text{CO}_2} / \delta T)_{P,X} = (h^+ - \bar{h}) / RT^2 \quad (5)$$

where, h^+ and \bar{h} are the molar enthalpy of CO_2 in the ideal gas state and the partial molar enthalpy of CO_2 , respectively. Henry's Law is then given by the expression:

$$\ln f_{\text{CO}_2} / X_{\text{CO}_2} = \ln H + \bar{v}(P - P_r) / RT + (\bar{h} - h^+) / R (1/T - 1/T_r) \quad (6)$$

and can be rearranged to yield:

$$X_{\text{CO}_2} = f_{\text{CO}_2} / H(P_r, T_r) \exp(-\bar{v}(P - P_r) / RT - \Delta h / R (1/T - 1/T_r)) \quad (7)$$

where Δh is the heat of solution of CO_2 given by $\bar{h} - h^+$ at P_r and $H(P_r, T_r)$ is the Henry's Law constant at P_r and T_r . At reference P and T , H is simply equal to $f_{\text{CO}_2}(P_r, T_r) / X_{\text{CO}_2}(P_r, T_r)$, making expression (6) identical with that used by Stolper et al., (1986) for CO_2 in albite melt.

Although the selection of P_r and T_r is totally arbitrary, it is important to consider that the value of the Henry's constant will be greatly affected by the selection of the reference P and T . It is, therefore, advantageous to select P_r and T_r such that the essence of the thermodynamic definition of the Henry's constant:

$$H \equiv \lim_{x \rightarrow 0} \frac{f}{x} \quad (8)$$

is preserved (i.e. the linear form of Henry's Law (2) is still obeyed). The advantage of this selection is not altogether altruistic. Specification of a reference P and T forces the least squares regression through the data collected at those physical conditions. Considering the error associated with any one given experimental point leads to the conclusion that an arbitrary selection of P_r and T_r may not produce the optimum value of H and, thus, lead to non-optimal values for \bar{v} and Δh .

With this in mind, we select a reference P, T, and X_{CO_2} which not only conforms to the linear form of Henry's Law but which has a Henry's constant ($f_{\text{CO}_2}(P_r, T_r)/X_{\text{CO}_2}(P_r, T_r)$) that most closely approximates the value of the linear Henry's constant of 1.937×10^6 bar. Experiment BF108 run at 2025 bars and 1050°C conforms nicely to these criteria and is chosen as reference. The complete physical conditions of BF108 are given in Table 4. Most notable is its value of $H(P_r, T_r)$ which is 1.967×10^6 bar; almost identical to the linear Henry's constant.

Table 4 gives the values for \bar{v} and Δh determined with a least squares regression. The uncertainties given are the standard error of the estimates. The partial molar volume at infinite dilution is determined to be $34.0 \pm 0.5 \text{ cm}^3/\text{mole}$. This compares favorably with the work of Spera and Bergman (1980) who use the data of Mysen et al., (1976) and Mysen (1976) to determine the partial molar volume of CO_2 in albite, jadeite and nepheline glasses ($35\text{--}30 \text{ cm}^3/\text{mole}$). These partial molar volumes are not directly comparable since the glasses were produced at high P and T ($1460^\circ\text{C} < T < 1620^\circ\text{C}$ and $10 \text{ kb} < P < 30 \text{ kb}$), were not rhyolitic in composition and contained large fractions of CO_2 dissolved as carbonate. A further complication is that the validity of the data presented by Mysen et al., (1976) has been called into question. Stolper et al., (1986) indicate problems with the experimental and analytical techniques of Mysen et al., (1986) as well as inconsistencies in the determinations of CO_2 and CO_3^{2-} in albite with their own IR measurements. The partial molar volume presented here deviates somewhat from Stolper et al., (1986) who determine a value of $28.6 \text{ cm}^3/\text{mole}$ for \bar{v} in albite melt. This value was determined with a regression through their data at roughly similar P and T to that of Mysen et.

al., (1986) and using the same analytical techniques as that used in this study.

One of the assumptions of the model is that \bar{v} is not a function of P. Krichevsky and Kasarnovsky (1935) suggest that \bar{v} may be assumed to follow a simple relation with P such as:

$$\bar{v} = \bar{v}^0 - \beta P \quad (9)$$

where \bar{v}^0 is the partial molar volume at 0 pressure and β is the coefficient of compressibility. Incorporation of this expression did little to improve the model and verified the initial assumption of the constancy of \bar{v} with P.

Equation 7 makes use of the CO₂ fugacity as well as the solubility data reported in Table 2 to determine the thermodynamic constants H , \bar{v} , and Δh . Obviously then, the least squares values determined for these constants depend upon the correct determination of f_{CO_2} as well as the solubility data. Although the HSMRK equation of state (EOS) of Kerrick and Jacobs (1981) was used for this purpose, it is important to investigate the effects of differing f_{CO_2} on the thermodynamic constants. For this purpose we redetermined H , \bar{v} , and Δh using the f_{CO_2} calculated with the Modified Redlich Kwong (MRK) equation of state of Holloway (1977). The values of these constant are given in Table 3. Most notable is the fact that the three constants are somewhat different, although, not radically, from those calculated previously. It is our opinion that the HSMRK model of Kerrick and Jacobs (1981) retrieves superior values of f_{CO_2} than that of the MRK model of Holloway (1977). The HSMRK model is more solidly grounded on theoretical considerations (1) use of the Carnahan and Starling (1972) Hard Sphere repulsion term, 2) attractive term resembles the virial expansion), and appears to retrieve CO₂ fugacities, in the temperature range under consideration, that are more consistent with the fugacity tables of Shmulovich and Shmonov (1978) than do the values of f_{CO_2} calculated with the MRK model (see Table 3 in Kerrick and Jacobs (1981)). For these reasons we prefer the values of the thermodynamic constants determined with the HSMRK than with the MRK.

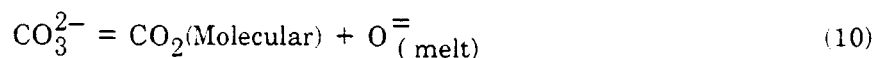
Two other considerations concerning the use of this model in relation to the calculation of CO₂ fugacity are pertinent to this discussion. First, since different equations of state yield different f_{CO_2} and hence different CO₂ solubility constants, the use of Equation 7 is restricted to CO₂

solubility determinations with either one of these equations of state. Thus, application of Equation 7 with CO_2 fugacities determined with a third EOS may yield erroneous CO_2 solubilities. The solubility constants need redetermination when the EOS of the fluid is changed. This sad fact is a function of the lack of accurate PVT data at high P and T for CO_2 which necessitates the use of EOS with extrapolation capabilities. Second, since different EOS yield differing solubility constants, the error on the constants reflect the error in the solubility measurements and experiments. The absolute values of these constants may, therefore, be somewhat outside the uncertainty values given. Caution is required not to put too much significance into the actual values of these constants.

Discussion

The Absence of Carbonate

The lack of detectable carbonate in CO_2 saturated rhyolite glasses at pressures up to 6.6 kbar is consistent with the trend of decreasing $\text{CO}_3^{2-}/\text{CO}_2(\text{Molecular})$ ratio with increasing silica activity. This trend has been observed by Fine and Stolper (1985) for glasses along the $\text{NaAlO}_2\text{-SiO}_2$ join. Although the added complication of CO gas is present, unpublished data from our lab on basalt, andesite and rhyodacite melts equilibrated with a graphite-CO- CO_2 fluid show the same trend with silica activity. The basaltic glasses contain only dissolved carbonate, whereas the andesite and rhyodacite contain both CO_3^{2-} and molecular CO_2 , with the latter increasing at the expense of the former, in the more evolved liquids. Rhyolite appears to complete this sequence with only dissolved $\text{CO}_2(\text{Molecular})$ present. This trend may well be due to the competition of CO_2 with Al for charge balancing cations such as Na (Brearley and Montana, 1988). This suggests that carbonate would be present in peralkaline rhyolites equilibrated at the same P and T as that investigated here. Since peralkaline rhyolites contain alkalis in excess of aluminum, charge balancing cations would be available for CO_3^{2-} complex formation without competition with Al. Irrespective of the mechanism, these observations clearly indicate that forward reaction in the equilibria



is favored with progressive evolution in the basalt rhyolite petrogenetic sequence.

The experiments presented here were all carried out at pressures below 6.6 kbar. We have no doubt that carbonate is present in these experimental glasses; albeit at a level below FTIR detection (roughly 25 ppm for the techniques presented here). A progressive increase in pressure above 6.6 kbars should eventually bring carbonate levels above IR detectability limits. This contention is supported by the data of Fine and Stolper (1985) which indicate the presence of carbonate in CO_2 undersaturated experiments on $\text{NaAlSi}_4\text{O}_{10}$ glass at 25 kbar.

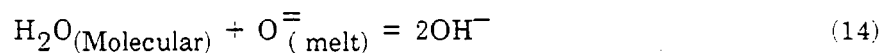
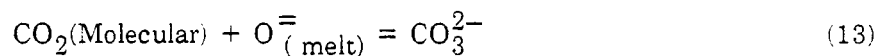
Application to Rhyolitic Volcanism

With the aid of the CO_2 solubility model, it is possible to extrapolate the results of this study to temperatures of rhyolitic volcanism in order to make estimates as well as predictions of CO_2 concentrations in magmas.

The fluid phase associated with rhyolitic magmatism usually contains a large if not dominant fraction of H_2O in the vapor phase. At a given P and T water will dissolve preferentially to CO_2 within the silicate melt. The heterogeneous equilibrium between fluid and magma with respect to both CO_2 and H_2O are:



The homogeneous equilibria within the melt are:



There are two basic unknowns in the formulation of these equilibria and those are the extent of CO_2 - H_2O non-ideality in the fluid phase, and the effect of dissolved H_2O and CO_2 on their mutual solubilities. Unfortunately, there is a paucity of thermochemical data on CO_2 - H_2O mixtures at high P and T necessitating reliance on the predictive capacities of reasonably formulated equations of state. The HSMRK equation of state of Kerrick and Jacobs (1981) predicts an extreme degree of non-ideality between mixtures of these two gases. For small X_{CO_2} the activity coefficient of

CO₂ is predicted to be quite high and the same is true for the activity coefficient of H₂O at small X_{H₂O}. This further complicates the situation since CO₂ can reach high degrees of dilution at magmatic conditions.

Currently, there is no consensus as to the affects of dissolved CO₂ and H₂O on their mutual solubilities. As a first approximation, these effects can be assumed to be negligible. In actuality, since total dissolved CO₂ is quite low, both in an absolute sense as well as relative to H₂O, it is more likely that the effect of water upon CO₂ will be more profound than the effects of CO₂ upon H₂O. If CO₂-H₂O concentrations are available for magmatic liquids, the CO₂ solubility model presented here together with temperature and H₂O solubility estimates can be used to estimate magmatic pressures.

Anderson et al., (1988) determined the H₂O and CO₂ concentrations in quartz melt inclusions from the plinian deposit of the Bishop Tuff. H₂O was determined to be between 5.3-5.8 wt% and CO₂ between 50 and 190 ppmw. Hildreth (1979) estimated a T of 725°C for the earliest deposits of the Bishop Tuff with the Fe-Ti oxide geothermometer. The P_{H₂O} capable of producing a rhyolitic liquid of 5.8 wt% H₂O can be estimated with the experimental data of Tuttle and Bowen (1960) to be ≈ 1800 bars. By an iterative process, we select a total pressure and determine the f_{CO₂} required to produce a melt of 190 ppm by weight CO₂. This can be checked against the HSMRK fluid model to search for a P_{CO₂} (or X_{CO₂}) that produces the CO₂ fugacity determined in the previous step. If the sum of P_{H₂O} and P_{CO₂} do not approximate the initial total pressure estimate, a new P is estimated and the process begins anew. Using the method just described, we determined a minimum P_{Total} (or actual P_{Total} if vapor saturation is assumed) for the top of the Bishop Tuff magma chamber of ≈ 2000 bars and an X_{H₂O} and P_{CO₂} of 0.90 and 200 bars, respectively. This is within the pressure range calculated by Hildreth and Spera (1974) for quartz, hypersthene and titanomagnetite equilibration within the Bishop Tuff.

Rhyolite vs Basalt

The data presented here on the solubility of CO₂ in rhyolite and the data of Stolper and Holloway (1988) on CO₂ solubility in basalt can be used together to estimate the relative

solubilities of the two compositions. The experimental data of Stolper and Holloway (1988) show that at 1200°C and 1000 and 1500 bars total CO₂ gas pressure the solubility of CO₂ in basalt is 390 and 577 ppm by weight, respectively. This translates into 565 and 836 ppm by mole (calculated on the basis of the oxides). Using the solubility model presented here, the corresponding CO₂ solubility in rhyolite is 745 and 1116 ppm by mole, respectively. This demonstrates that on a molar basis CO₂ solubility in rhyolite is slightly higher than that in basalt; a situation which is true on a weight percent basis as well.

Based upon these calculations, it would appear that there are two main differences in the comparison of CO₂ solubility in basalt and rhyolite. First, the solubility of CO₂ in rhyolite is somewhat greater than that in basalt at the same P and T. This demonstrates that as far as total CO₂ is concerned the decrease in silica activity between rhyolite and basalt does not cause an increase in CO₂ solubility. This goes against the conclusions of many workers that CO₂ solubility decreases with increasing silica content (Eggler and Rosenhauer, 1978; Holloway et al., 1976; Mysen et al., 1976; Carmichael et al., 1974; Eggler, 1973). We trust the accuracy of our conclusions over that of the above authors since: 1) our analytical technique is essentially identical to that of Stolper and Holloway (1988), 2) they are based upon direct CO₂ concentrations and not implied from phase equilibria or other information and 3) the repudiation of the accuracy of beta track autoradiography for determination of CO₂ concentrations (Tingle and Aines, 1988) calls into question conclusions that are based upon data generated by this technique (eg. Mysen et al., 1976). At this time, however, we can only make this comparison between basalt and rhyolite at pressures below 1500 bars. Second, the difference in CO₂ solubility between rhyolite and basalt is manifested in its mode of speciation. At low pressure CO₂ dissolves in basalt exclusively as carbonate whereas in rhyolite it dissolves exclusively in the molecular form.

Conclusions

1. CO₂ solubility in rhyolite at 1050°C follows a linear Henry's Law behavior to pressures of roughly 2300 bars. Above this pressure CO₂ solubility rapidly becomes non-ideal and deviates

from the linear form of Henry's Law.

2. Results of experiments along the 950°C, 1050°C and 1150°C isotherm show a decrease in CO₂ solubility with increasing temperature.

3. Water concentrations below 0.30 wt % do not appear to affect either the speciation or solubility of CO₂ in rhyolite melt.

4. The diffusion of CO₂ into rhyolite appears to be the main mechanism for CO₂(fluid)-rhyolite equilibration. The diffusion of CO₂ into rhyolite is slow and the diffusion coefficient at 1050°C has been approximated to be roughly 10^{-7.6} cm²/sec.

5. CO₂ solubility data can be described by an extended Henry's Law model that takes into account the affect of pressure and temperature. These are related to the partial molar volume at infinite dilution and the heat of solution of molecular CO₂ in rhyolite melt. \bar{v} and Δh were determined to be 34.0 ± 0.5 cm³ and -15.9 ± 3.9 kJ/mole respectively.

6. CO₂ dissolves in rhyolite melt solely in the molecular form at least down to FTIR detectability limits for CO₃²⁻. This apparently follows the general trend of greater CO₂(Molecular)/CO₃²⁻ ratios through the sequence basalt, andesite, rhyodacite, rhyolite (with basalt showing no detectable molecular CO₂).

7. CO₂ solubility data, along with H₂O solubility data and T estimates, can be used to make P_{Total}, P_{CO₂} and X_{H₂O} estimates from melt inclusion volatile determinations. This has been done for the plinian deposits of the Bishop Tuff using the melt inclusion data of Anderson et al., (1988). A P_{Total}, P_{CO₂} and X_{H₂O} of 2000 bars 200 bars and 0.90 were determined for a magmatic T of 725°C.

8. A comparison of CO₂ solubility in rhyolite and that in basalt at low pressures and 1200°C shows that CO₂ is slightly more soluble in rhyolite than in basalt. The difference in solubility between the two magma types is most pronounced in their speciation within the silicate liquid: CO₂ dissolves in basalt as carbonate complexes, and in rhyolites as molecular CO₂.

References

- Anderson A.T., Skirius C., Williams S.N., Drit T., Newman S. and Stolper E. (1988) H_2O , CO_2 , Cl and gas in Bishop Rhyolite. *EOS* 69, 529.
- Brearley M. and Montana A. (1988) The effect of CO_2 on the viscosity of silicate liquids at high pressure. *Geochim. Cosmochim. Acta* (submitted).
- Carmichael I.S.E., Turner F.J. and Verhoogen (1974) "Igneous Petrology." McGraw Hill, New York, pp. 739.
- Crank J. (1985) "The Mathematics of Diffusion." Clarendon Press, Oxford, pp. 414.
- CRC Handbook of Chemistry and Physics (1981), ed. Weast R.C. and Astle M.J..
- Dixon T.E., Stolper E. and Delaney J.R. (1988) Infrared spectroscopic measurements of CO_2 and H_2O in Juan de Fuca Ridge basaltic glasses. *Earth Planet. Sci. Lett.* 90, 87-104.
- Eggler D.H. (1973) Role of CO_2 in melting processes in the mantle. *Carnegie Inst. Washington Yearb.* 72, 457-467.
- Eggler D.H. and Rosenhauer M. (1978) Carbon dioxide in silicate melts: II. Solubilities of CO_2 and H_2O in $CaMgSi_2O_6$ (diopside) liquids and vapors at pressures to 40 kb. *Am. J. Sci.* 278, 64-94.
- Fine G. and Stolper E. (1985) The speciation of carbon dioxide in sodium aluminosilicate glasses. *Contrib. Mineral. Petrol.* 91, 105-121.
- Fine G. and Stolper E. (1986) Dissolved carbon dioxide in basaltic glasses: concentrations and speciation. *Earth Planet. Sci. Lett.* 76, 263-278.
- Gerlach T.M. (1986) Exsolution of H_2O , CO_2 and S during eruptive episodes at Kilauea Volcano, Hawaii. *J. Geophys. Res.* 91, 12,177-12,185.
- Hildreth W. (1979) The Bishop Tuff: Evidence for the origin of compositional zonation in silicic magma chambers. *Geological Society of America Special Paper* 180, 43-75.
- Hildreth W. and Spera F. (1974) Magma Chamber of the Bishop Tuff: Gradients in T, P_{Total} , and P_{H_2O} . *Geol. Soc. Am. Abst. Program.* 6, 795.
- Holloway J.R. (1977) Fugacity and activity of molecular species in supercritical fluids, in Fraser

- D.G. ed., *Thermodynamics in Geology*: Dordrech-Holland, D. reidel Publishing Co., p. 161-181.
- Holloway J.R., Mysen B.O. and Eggler D.H. (1976) The solubility of CO_2 in liquids on the join $\text{CaO-MgO-SiO}_2\text{-CO}_2$. *Carnegie Inst. Washington Yearb.* 75, 626-631.
- Johnson M.C. and Rutherford M.J. (1989) Experimentally determined conditions in the Fish Canyon Tuff, Colorado, magma chamber. *J. Petrol.*, (in press).
- Kerrick D.M. and Jacobs G.K. (1981) A modified Redlich-Kwong equation for H_2O , CO_2 and $\text{H}_2\text{O-CO}_2$ mixtures at elevated pressures and temperatures. *Am. Jour. Sci.* 281, 735-767.
- Krichevsky I.R. and Kasarnovsky J.S. (1935) Thermodynamical calculations of solubilities of nitrogen and hydrogen in water at high pressures. *J. Am. Chem. Soc.* 57, 2168-2171.
- Mysen B.O. (1976) The role of volatiles in silicate melts: Solubility of CO_2 and H_2O in feldspar, pyroxene and feldspathoid melts to 30 kbar. *Am. J. Sci.* 276, 969-996.
- Mysen B.O., Eggler D.H., Seitz M.G. and Holloway J.R. (1976) Carbon dioxide in silicate melts and crystals: Part I Solubility measurements. *Am. J. Sci.* 276, 455-479.
- Newman S., Stolper E.M. and Epstein S. (1986) Measurement of water in rhyolitic glasses: Calibration of an infrared spectroscopic technique. *Am. Mineral.* 71, 1527-1541.
- Rai S.C., Sharma S.K., Muenow D.W., Matson D.W. and Byers C.D. (1983) Temperature dependence of CO_2 solubility in high pressure quenched glasses of diopside composition. *Geochim. Cosmochim. Acta* 47, 953-958.
- Roedder E. (1965) Liquid CO_2 inclusions in olivine-bearing nodules and phenocrysts from basalts. *Am. Mineral.* 50, 1746-1782.
- Rutherford M.J., Sigurdsson H., Carey S. and Davis A. (1985) The May 18, 1980, eruption of Mount St. Helens, 1, Melt composition and experimental phase equilibria. *J. Geophys. Res.* 90, 2929-2947.
- Sharma S.K., Hoering T.C. and Yoder H.S. (1979) Quenched melts of akermanite compositions with and without CO_2 —Characterization by Raman spectroscopy and gas chromatography. *Carnegie Inst. Washington Yearb.* 78, 537-542.

- Shmulovich K.I. and Shmonov V.M. (1978) "Tables of the Thermodynamic Properties of Gases and Liquids (Carbon Dioxide)" (In Russian). Gosdarstvennaya Sluzhba Standartnykh Dannykh, pp. 165.
- Silver L. and Stolper E. (1989) Water in albitic glasses. *J. Petrol.* (submitted).
- Spera F.J. and Bergman S.C. (1980) Carbon dioxide in igneous petrogenesis: I. Aspects of dissolution of CO₂ in silicate liquids. *Contrib. Mineral. Petrol.* 74, 55-60.
- Stolper E. (1982) Water in silicate glasses: An infrared spectroscopic study. *Contrib. Mineral. Petrol.* 81, 1-17.
- Stolper E., Fine G., Johnson T. and Newman S. (1987) Solubility of carbon dioxide in albitic melt. *Am. Mineral.* 72, 1071-1085.
- Stolper E. and Holloway J.R. (1988) Experimental determination of the solubility of carbon dioxide in molten basalt at low pressure. *Earth Planet. Sci. Lett.* 87, 397-408.
- Tingle T.N. and Aines R.D. (1988) Beta track autoradiography and infrared spectroscopy bearing on the solubility of CO₂ in albite melt at 2 GPa and 1450°C. *Contrib. Mineral. Petrol.* 100, 222-225.
- Tuttle O.F. and Bowen N.L. (1960) "Origin of Granite in Light of Experimental Studies in the System NaAlSi₃O₈-KAlSi₃O₈-SiO₂-H₂O," The Geological Society of America Memoir 74, pp. 153.
- Watson E.B., Sneeringer M.A. and Ross A. (1982) Diffusion of dissolved carbonate in magmas: experimental results and applications. *Earth Planet. Sci. Lett.* 61, 346-358.

Table 1

Oxide	Wt %		CIPW Norm	
SiO ₂	76.45	(0.24)	<i>q</i>	33.12
TiO ₂	0.08	(0.05)	<i>or</i>	28.22
Al ₂ O ₃	12.56	(0.13)	<i>ab</i>	35.66
Fe ₂ O ₃	N.D	N.D.	<i>an</i>	1.24
FeO	1.02	(0.07)	<i>ne</i>	0.00
MnO	0.08	(0.07)	<i>lu</i>	0.00
MgO	0.06	(0.02)	<i>di</i>	0.00
CaO	0.25	(0.06)	<i>ol</i>	0.00
Na ₂ O	4.21	(0.11)	<i>mt</i>	0.00
K ₂ O	4.78	(0.21)	<i>il</i>	0.15
<hr/>				
Total	99.48			

Electron microprobe analysis of starting material VNM50-15 along with its CIPW Norm. All iron is calculated as FeO. Brackets indicate one standard deviation (1σ) on 6 microprobe analyses.

Experimental Results

Run # (BF)	Dur (hrs)	P (bars)	f_{CO_2} (bars)	d (μm)	Abs (2350 cm^{-1})	CO ₂ (ppmw)	CO ₂ (ppmm)	Abs (3570 cm^{-1})	H ₂ O (ppmw)	H ₂ O (ppmm)
T=950°C										
134	69	1,010	1,315	146	0.43958	597	878	0.23667	1,244	4,471
130	48	1,993	3,509	163	1.17733	1,433	2098	0.48750	2,295	8,207
T=1050°C										
111	15	504	566	375	0.35583	188	277	0.48583	994	3,578
123	46	1,000	1,291	275	0.68083	491	723	0.40500	1,130	4,063
124	42	1,500	2,241	248	0.99600	797	1,173	0.31917	988	3,553
108	62	2,025	3,531	160	0.98533	1,221	1,795	0.24750	1,187	4,263
128	43	2,490	4,977	121	0.94375	1,547	2,270	0.25600	1,624	5,820
139	70	3,529	9,545	157	1.59500	2,015	2,951	0.40167	1,963	7,022
153	96	4,324	14,699	103	1.35357	2,605	3,816	0.22167	1,652	5,911
153C	96	4,324	14,699	104	1.50320	2,867	4,198	0.21809	1,609	5,756
145	96	5,496	25,913	141	2.06500	2,905	4,246	0.38683	2,106	7,520
148	75	6,612	42,862	100	1.87083	3,711	5,405	0.35938	2,758	9,814
T=1150°C										
136	36	2,029	3,473	131	0.74333	1,125	1,658	0.10042	588	2,117
149	96	3,487	8,941	136	1.22750	1,790	2,632	0.16667	941	3,380
131	16	4,500	15,192	174	2.05000	2,337	3,434	0.20333	897	3,220

Table 3

CO₂ Diffusion in Rhyolite at 1050°C

Exp (BF)	P (bar)	t (sec)	Rim CO ₂ (ppmm)	Core CO ₂ (ppmm)	a (cm)	Dt/a ²	Log ₁₀ D
123	1,000	165,600	723	273	0.168	0.163	-7.56
124	1,500	151,200	1,173	342	0.140	0.140	-7.74
128	2,490	154,800	2,270	759	0.164	0.145	-7.60
Av							-7.63

Core and rim concentrations of CO₂ and relevant parameters for calculation of the diffusion coefficient of CO₂ in rhyolitic melt. Melt geometry is assumed to approximate a cylinder. a is the distance between measure rim and core concentrations, t is the duration of the experiment and the dimensionless parameter Dt/a² is taken from Crank (1985).

Table 4
Solution Model Parameters

$P_r = 2025 \text{ bars}; \quad T_r = 1050^\circ\text{C}$

f_{CO_2} Model	$H(P_r, T_r)$ (bars)	\bar{v} (cm ³ /mole)	Δh (kJ/mole)
HSMRK	1.967×10^6	34.0 ± 0.5	-15.9 ± 3.9
MRK	1.841×10^6	31.2 ± 0.5	-12.9 ± 4.1

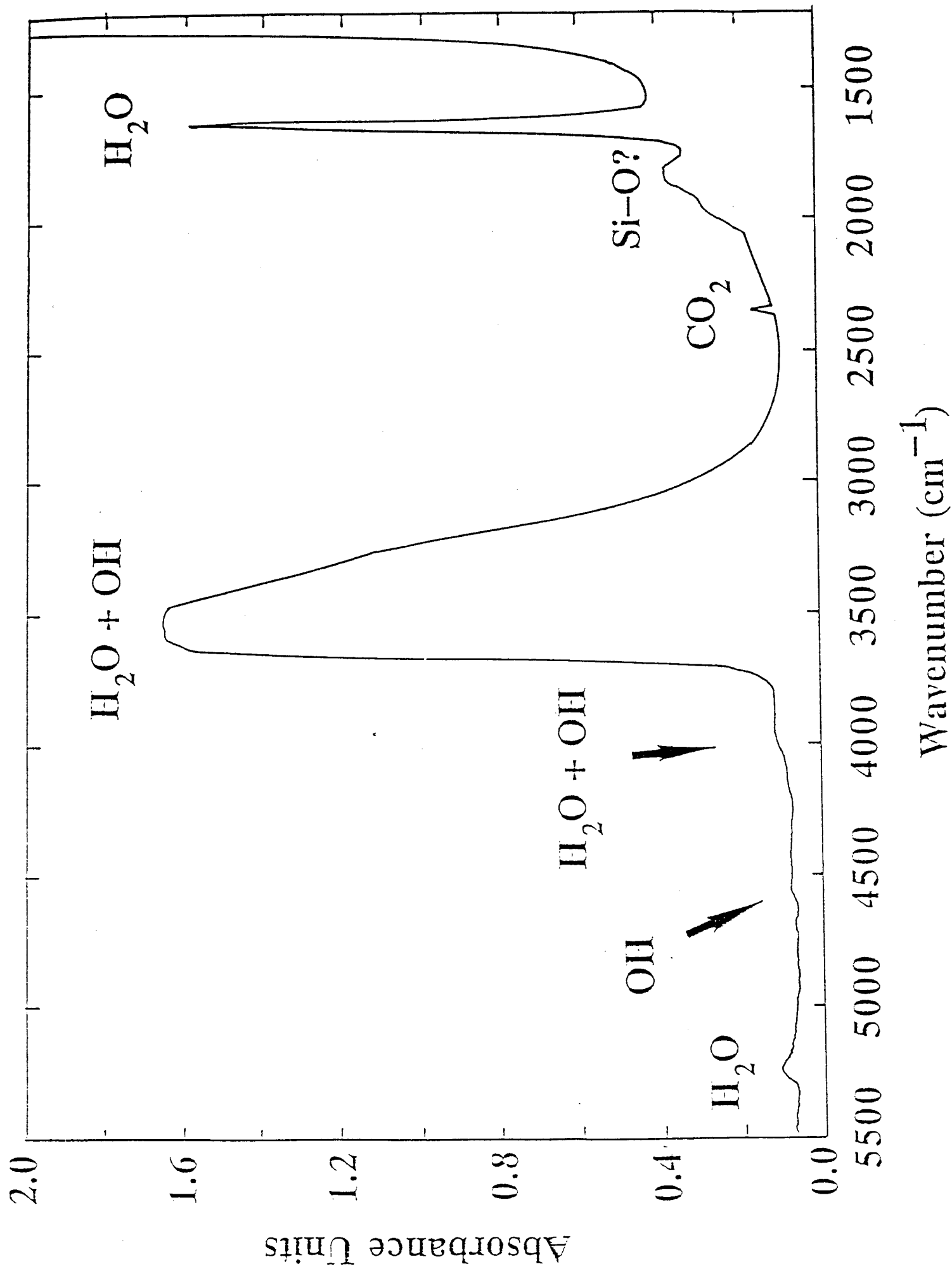


Figure 1

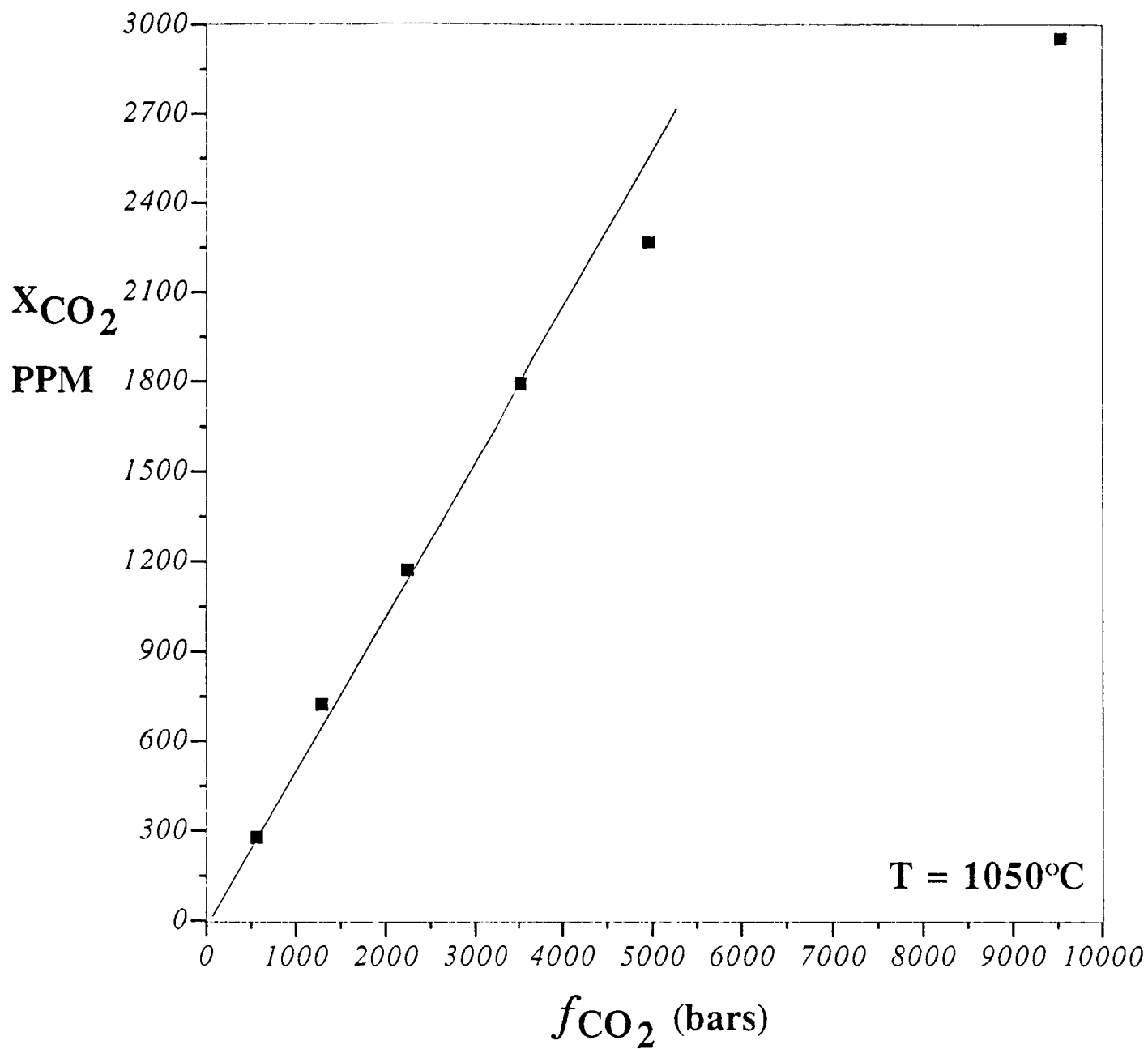


Figure 2

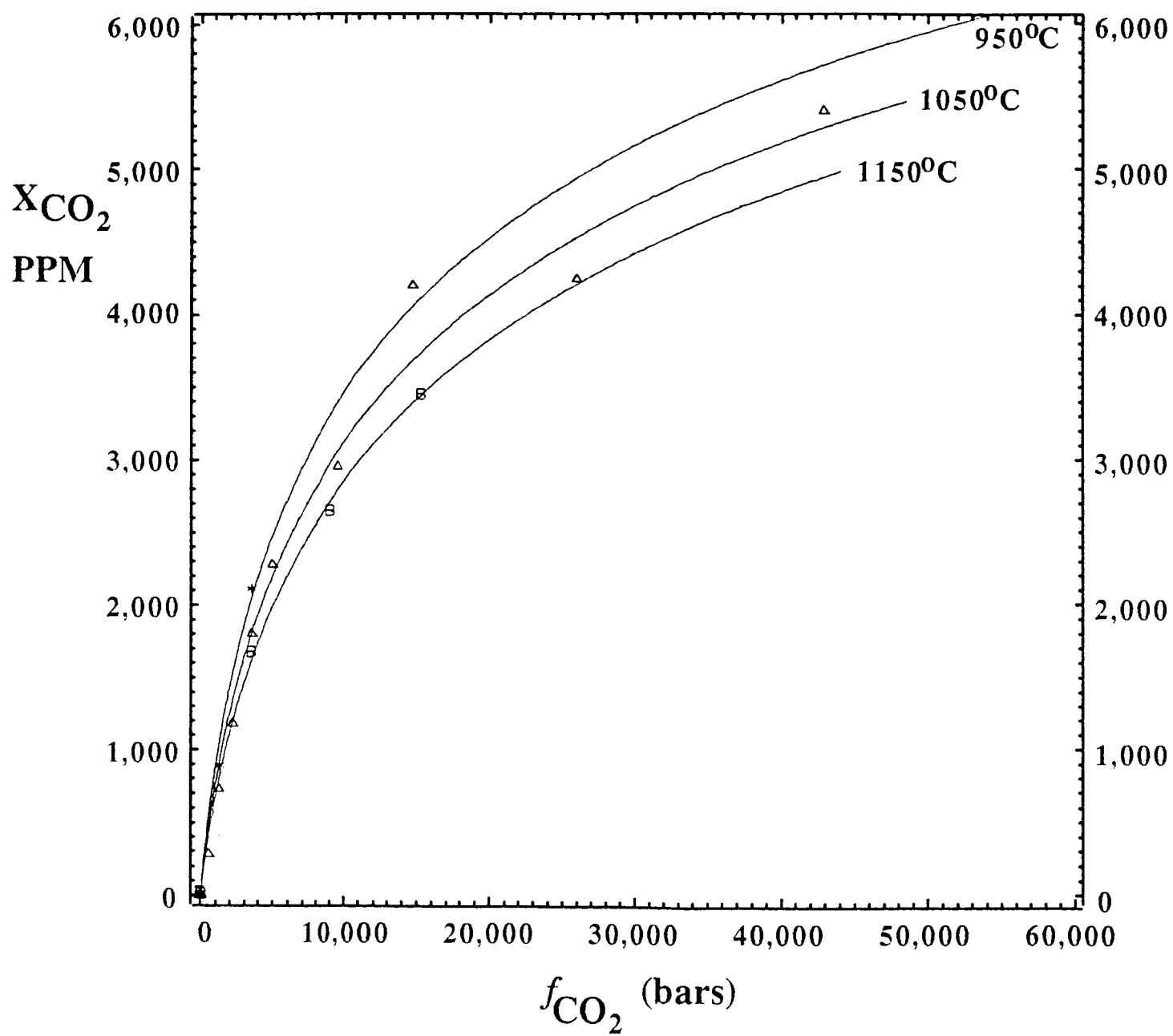


Figure 3

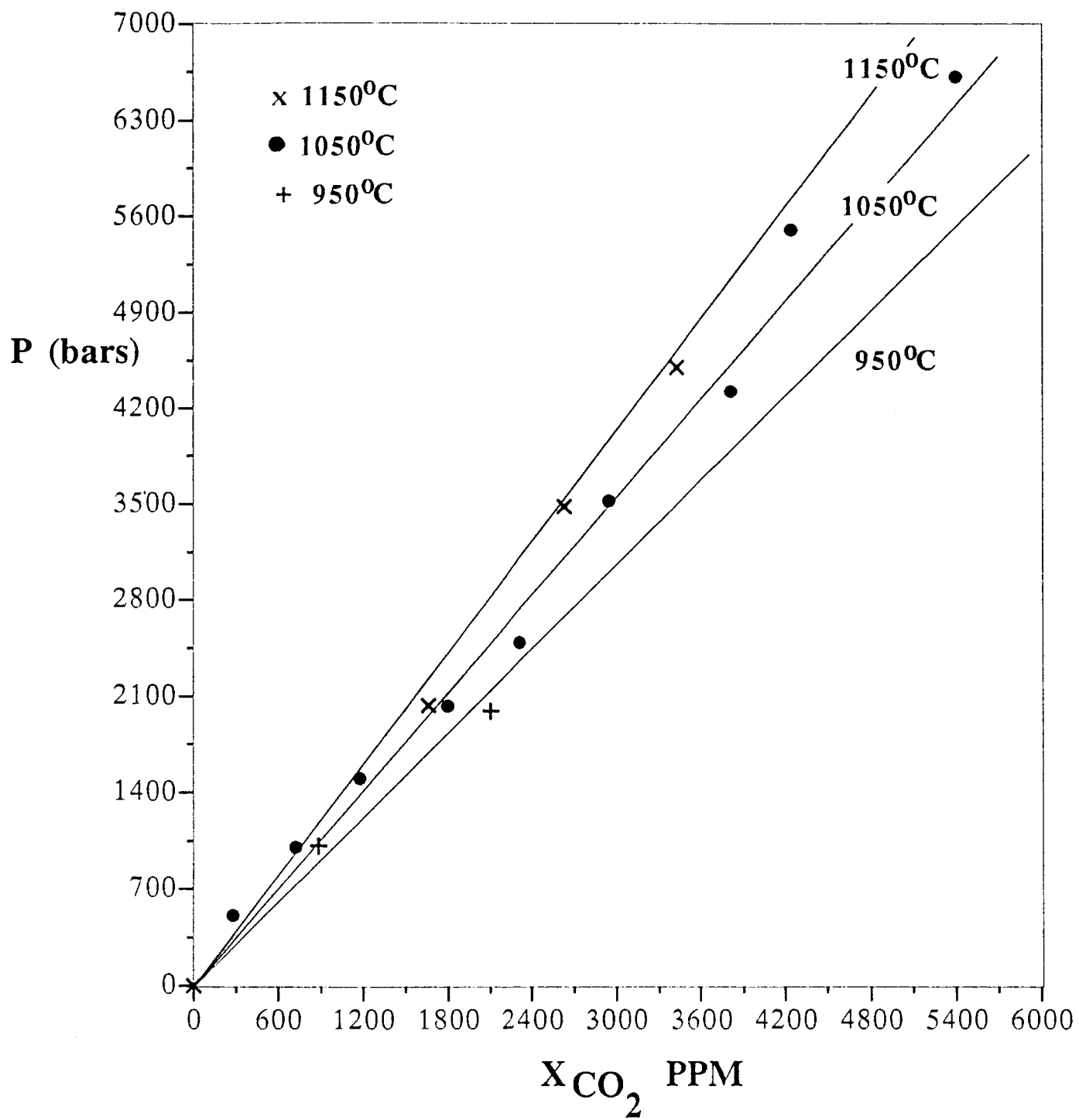


Figure 4

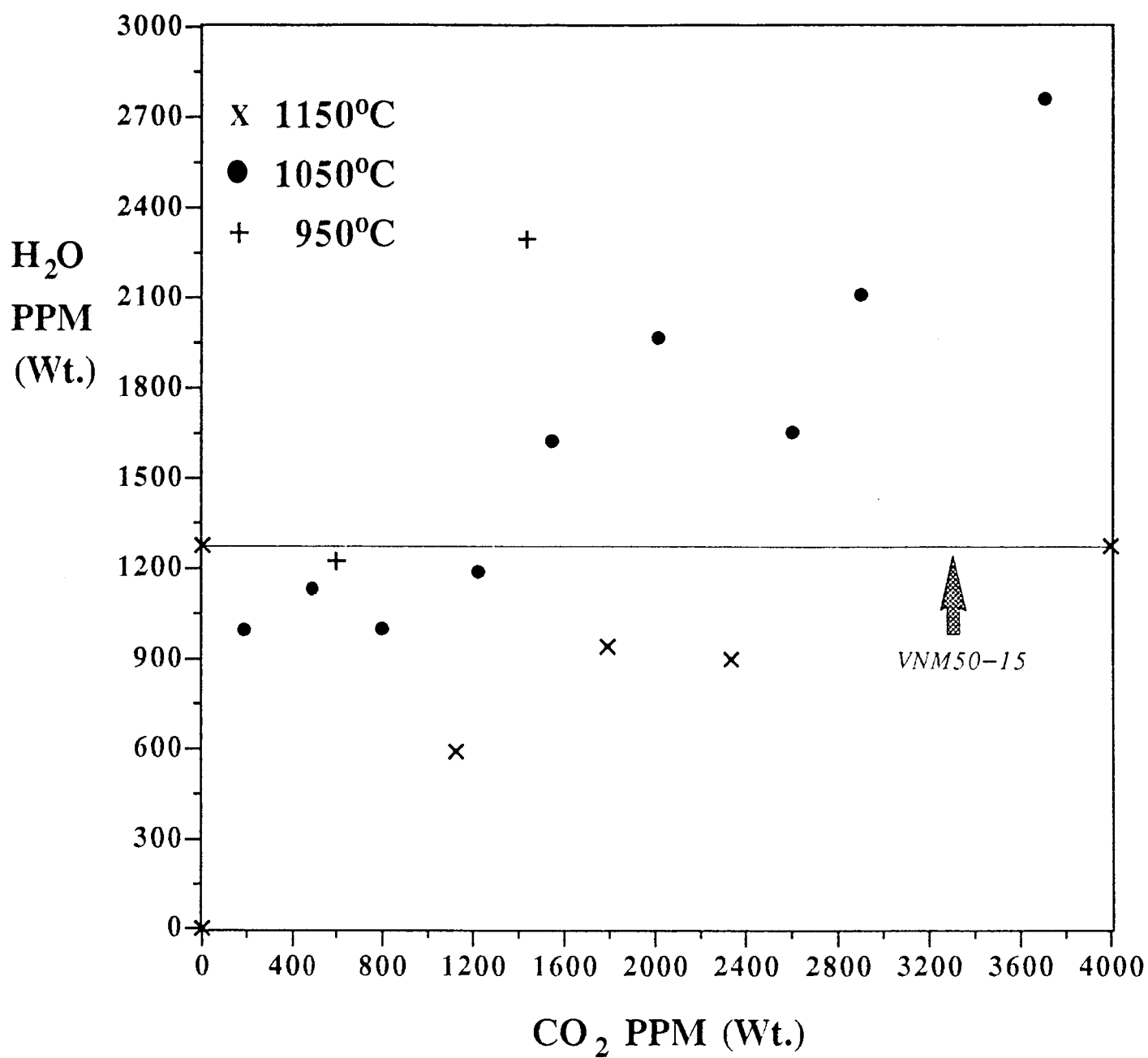


Figure 5

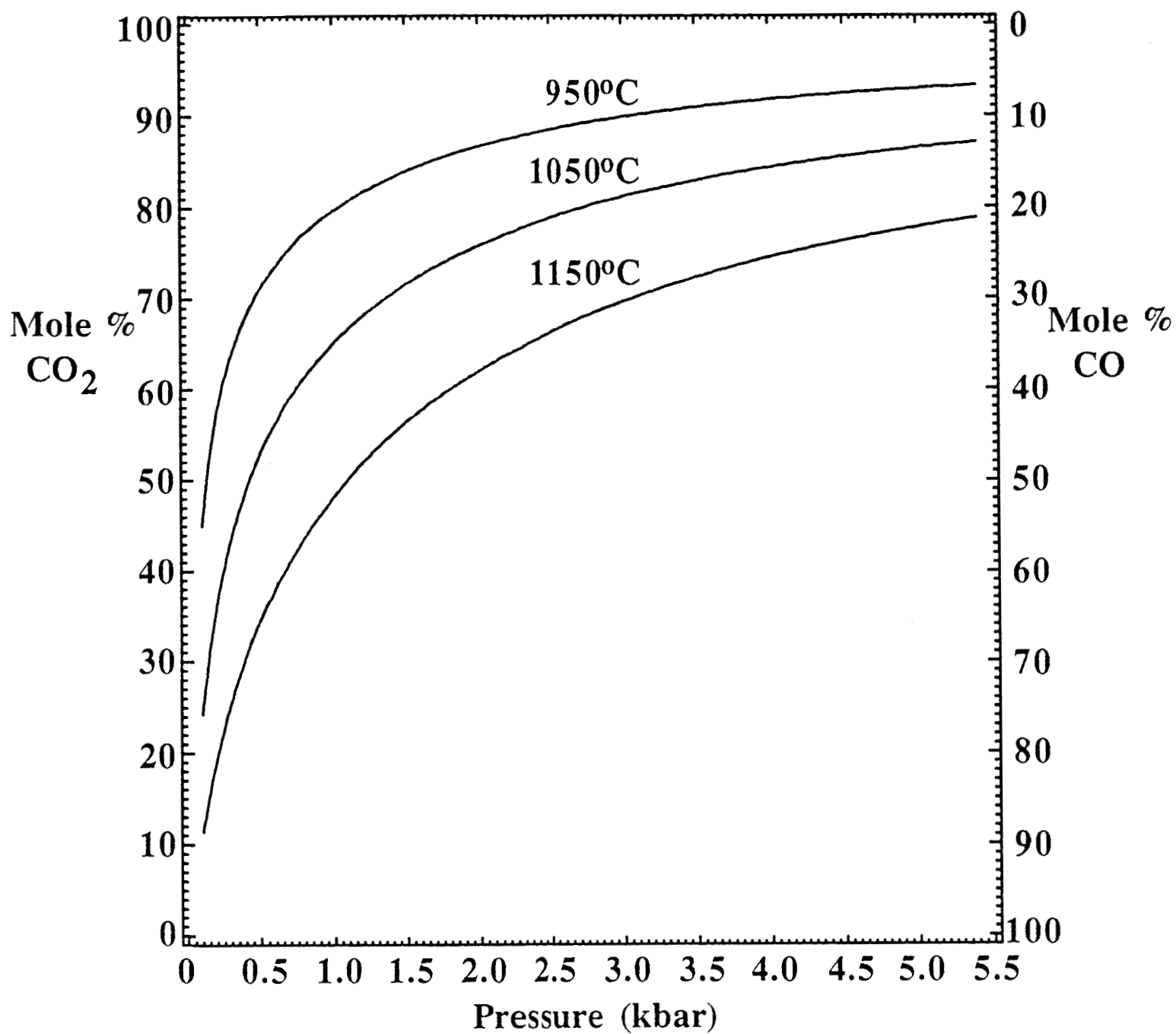


Figure 6